Anomalous Rheological Behavior of Ordered Phases of Block Copolymers. 1

Takao Ohta,† Yoshihisa Enomoto,‡ James L. Harden,§ and Masao Doi*,§

Department of Physics, Faculty of Science, Ochanomizu University, Bunkyo-ku, Tokyo 112, Japan, Department of Physics, Nagoya Institute of Technology, Showa-ku, Nagoya 466, Japan, and Department of Applied Physics, Nagoya University, Chikusa-ku, Nagoya 464, Japan

Received March 5, 1993; Revised Manuscript Received June 7, 1993

ABSTRACT: Computer simulation is carried out for microphase-separated diblock copolymers under applied shear deformation. A mesophase of hexagonally ordered cylindrical domains is considered, and shear strains are applied perpendicular to the cylinder axes. Rheological responses and structural changes of the system under oscillatory and step-shear strains are studied by using a cell dynamic approach. For small strains, the usual behavior of ordered viscoelastic solids is seen, while for large strains, anomalous behavior is observed, including (i) in the case of oscillatory shears, a nonlinear stress response which is out of phase with the applied strain in the low frequency limit and (ii) in the case of step-shear, a double stress relaxation process in which the stress first approaches a pseudoequilibrium value and then much later relaxes further toward the final equilibrium value. This anomalous behavior is shown to be due to the slippage of lattice planes.

1. Introduction

Ordered phases of block copolymers exhibit many unusual and interesting properties due to the existence of a characteristic length associated with the ordering which is neither microscopic nor macroscopic.[1-4] In particular, these materials are solidlike on mesoscopic length scales, even when their constituents are in the molten state. One important consequence of this is that the mechanical and rheological properties of these ordered mesophases on sufficiently long time scales are rather different from those of the corresponding disordered phases.

Both dynamics and statics of the microphase-separated block copolymer system have been studied experimentally by many groups.[1-13] Unusual dynamic features observed in experiments include a rather dramatic nonlinear response to very low frequency oscillatory shear strains, plastic flow with a true yield stress,[5-8] and anomalous frequency scaling of the linear dynamic viscoelastic modulus $G^*(\omega)$.[9,10] Theoretical understanding of the structure and equilibrium properties of copolymer mesophases had advanced significantly in recent years.[14-20] On the other hand, the theory for the dynamics of the ordered phase has not been developed very far.

The dynamics of the ordered phase of block copolymers have two aspects. One is the problem of individual chains: how a copolymer chain can move in a nonuniform environment. The other is the problem of the structural change of mesophases: how the domains change their shape and relative position in response to externally applied perturbations. The former problem has been studied by several groups from the point of view of the relaxation of interdomain chain entanglements,[21,22] while the latter problem has not been tackled so far, with a few exceptions.[22,23]

In this paper, we shall attack the latter problem by computer simulation. We consider a microphase-separated state of AB-diblock copolymers and study its dynamic response to shear deformation. We consider the case that the mesophase is a defect-free hexagonal array of cylindrical domains and restrict our attention to shear deformations applied perpendicularly to the axes of the cylinders. Thus the problem we consider is effectively two-dimensional. We study how a shear strain deforms the domains and lattice structure and how such deformation is reflected in the rheological properties. We show that the rheological properties are quite different from both those of homogeneous copolymer phases and of linear viscoelastic crystalline solids. In particular, we show that nonlinear rheological response to applied step-shear and low frequency oscillatory shear strains of sufficient magnitude occur and that this anomalous behavior is correlated with the relative slipping of lattice planes.

At this point, a caution must be mentioned if this simulation is compared with experimental results. In general the rheological properties of ordered phases are very sensitive to defects. This has been demonstrated by recent experiments,[12,13] and also in our simulation. Therefore, direct comparison between simulation and experiment is not meaningful if the defect structure is not controlled. Due to the periodic boundary condition used in the simulation, the system studied here includes much less defects than real systems. Experimentally, the defect of the mesophases can be reduced by applying oscillatory shear strain of sufficient magnitude and duration.[12,13] The present simulation can be compared with such a system.

The organization of this paper is as follows. In section 2, we present a model equation for the dynamics of microphase-separated copolymers under applied shear flow. In section 3, we describe the cell dynamics simulation technique employed in this work and provide the details of the equilibrium mesophase characteristics and shear flows studied. In section 4, we show the results of the simulation for the cases of applied oscillatory and step-shear strains. Finally, in section 5, we summarize and discuss our findings, and their relevance to experimental studies of the rheology of microphase-separated block copolymer systems. A preliminary result of the present simulation has already been published.[24]

2. Model

Since our purpose here is to study the effect of the deformation of domains, we do not consider the motion of individual chains. The characteristic time of chain motion is much shorter than the time scale of the structural

* To whom correspondence should be addressed.
† Ochanomizu University.
‡ Nagoya Institute of Technology.
§ Nagoya University.

0024-9297/93/2226-4928$04.00/0 © 1993 American Chemical Society

change of domains. So, chain conformations may be assumed to be in equilibrium for a given domain conformation. In order to avoid additional complications, we assume that microscopic properties such as the Kuhn statistical segment length and the chain flexibility of the two types of copolymer constituents are identical. Hence the two blocks are distinguishable only by the nature of interaction. Furthermore, we do not take account of the possible long range hydrodynamic effects.

Thus we describe the state of the block copolymer mesophase by the local volume fraction of A and B segments, $\phi_A(\boldsymbol{r})$ and $\phi_B(\boldsymbol{r})$. We assume that the system is incompressible ($\phi_A(\boldsymbol{r}) + \phi_B(\boldsymbol{r}) = 1$), so that the state of the system is described by a single order parameter

$$\psi(\boldsymbol{r}) = \phi_A(\boldsymbol{r}) - \phi_B(\boldsymbol{r}) \tag{2.1}$$

Due to mass conservation of A and B species, the spatial average of $\psi(\boldsymbol{r},t)$ is determined solely by the block ratio $f \equiv N_A/(N_A + N_B)$ via

$$\bar{\psi} \equiv \frac{1}{V}\int d\boldsymbol{r}\, \psi(\boldsymbol{r}) = 2f - 1 \tag{2.2}$$

where N_A and N_B are respectively the degrees of polymerization of A and B blocks.

For the dynamics of $\psi(\boldsymbol{r},t)$, we assume the standard time dependent Ginzburg Landau equation. If there is no macroscopic flow, this is written as

$$\frac{\partial \psi}{\partial t} = M\nabla^2 \frac{\delta H\{\psi\}}{\delta \psi} \tag{2.3}$$

Here M is a transport coefficient, and $H\{\psi\}$ is the free energy functional of the order parameter field $\psi(\boldsymbol{r})$ in units of the thermal energy k_BT. Ohta and Kawasaki[18] calculated $H\{\psi\}$ using a mean-field approximation and proposed that $H\{\psi\}$ for block copolymers can essentially be written as a sum of two terms: a short range interaction term $H_S\{\psi\}$ and a long-range interaction term $H_L\{\psi\}$,

$$H\{\psi\} = H_S\{\psi\} + H_L\{\psi\} \tag{2.4}$$

$H_S\{\psi\}$ has the same form as that for polymer blends:[25,26]

$$H_S\{\psi\} = \int d\boldsymbol{r}\left[W(\psi) + \frac{1}{2}D(\nabla\psi)^2\right] \tag{2.5}$$

where $W(\psi)$ is a function of ψ with two local minima, whose explicit form will be given later, and where the term $D(\nabla\psi)^2$ represents the free energy cost for spatial composition inhomogeneity (D scales with the Kuhn statistical segment length b as $D \propto b^2$). On the other hand, $H_L\{\psi\}$ is obtained from the long range interaction potential $G(\boldsymbol{r})$ which is the solution of $\nabla^2 G(\boldsymbol{r} - \boldsymbol{r}') = -\delta(\boldsymbol{r} - \boldsymbol{r}')$ as

$$H_L\{\psi\} = \frac{\alpha}{2}\int d\boldsymbol{r}\int d\boldsymbol{r}'\, G(\boldsymbol{r} - \boldsymbol{r}')[\psi(\boldsymbol{r}) - \bar{\psi}][\psi(\boldsymbol{r}') - \bar{\psi}] \tag{2.6}$$

where $\alpha \propto [Nbf(1-f)]^{-2}$ with a constant of proportionality that is of order unity and $N = N_A + N_B$ is the total copolymer degree of polymerization.

The above form of the free energy functional is an approximation for the exact power series expansion of the free energy with respect to $\psi(\boldsymbol{r})$. The exact form contains higher order, long range couplings of $\psi(\boldsymbol{r})$ and a much more involved form of $G(\boldsymbol{r})$. However, as it was demonstrated by Ohta and Kawasaki,[18] this form of the free energy reproduces many essential features of block copolymer mesophase behavior, including (i) the two-thirds power law for the domain size R in the strong segregation limit ($R \propto N^{2/3}$) and (ii) the appropriate structural transitions of the mesophases when the block ratio f is varied. Furthermore, Bahiana and Oono[27] conducted a computer simulation based on this free energy and showed that the microphase-separated structures are actually formed. Therefore, although the above expression for the free energy is approximate, we believe that it describes the essential physics of the ordered phase.

In the present paper we consider the case that there is a macroscopic shear flow, the velocity field of which is given by

$$v_x(\boldsymbol{r}) = \dot{\gamma}(t)y \qquad v_y = v_z = 0 \tag{2.7}$$

where the shear rate $\dot{\gamma}(t)$ is a given function of time. Under such a flow field, the time evolution equation for $\psi(\boldsymbol{r},t)$ given in eq 2.3 acquires a convective term and becomes

$$\frac{\partial \psi}{\partial t} + \nabla\cdot(\boldsymbol{v}\psi) = M\nabla^2 \frac{\delta H\{\psi\}}{\delta \psi} \tag{2.8}$$

In the simulation, we will choose the coordinate system so that the x-direction is parallel to a basis vector of the ordered hexagonal lattice formed by the equilibrium mesophase. Substituting eqs 2.5–2.7 into eq 2.8, we have

$$\frac{\partial \psi}{\partial t} = -\dot{\gamma}y\frac{\partial \psi}{\partial x} + M\nabla^2[-D\nabla^2\psi + F(\psi)] - M\alpha(\psi - \bar{\psi}) \tag{2.9}$$

where $F(\psi) \equiv dW/d\psi$. Notice that due to the Laplacian in eq 2.3, the long range term (the term proportional to α) becomes local in the equation of motion. This is the most advantageous feature of our model for computer simulation. If we set $\alpha = 0$, eq 2.9 becomes the same as that used previously in the study of the macrophase separation of binary blends under shear flow.[28]

Given the structure of the deformed mesophase, the stress can be calculated by the following formula derived in ref 29.

$$\sigma_{\alpha\beta} = -k_BT\frac{D}{V}\int d\boldsymbol{r}\frac{\partial \psi}{\partial r_\alpha}\frac{\partial \psi}{\partial r_\beta} + k_BT\frac{\alpha}{V}\int d\boldsymbol{r}\int d\boldsymbol{r}'\, r_\beta \frac{\partial G(\boldsymbol{r})}{\partial r_\alpha}\psi\left(\boldsymbol{r}' + \frac{\boldsymbol{r}}{2}\right)\psi\left(\boldsymbol{r}' - \frac{\boldsymbol{r}}{2}\right) \tag{2.10}$$

In the present study, we consider two types of shear flow. One is oscillatory shear, for which the shear strain is given by

$$\gamma(t) = \Gamma \sin(\omega t) \tag{2.11}$$

and the other is step-shear, defined by

$$\gamma(t) = \begin{cases} 0 & \text{for } t < 0 \\ \gamma & \text{for } t > 0 \end{cases} \tag{2.12}$$

For these shears, we study how the domains are deformed and displaced and how this is reflected in the stress tensor.

3. Method of Simulation

A cell dynamic version of eq 2.3 has been introduced by Oono and Puri[30] and by Bahiana and Oono.[27] Here we follow their procedure to simulate eq 2.9. We consider a $L \times L$ square lattice of cell size a and define the concentration $\psi(\boldsymbol{n},t)$ for each cell at the lattice point $\boldsymbol{n} = (n_x,n_y)$, where n_x and n_y are integers between 1 and L. The Laplacian ∇^2 is then transformed as

$$\nabla^2 X \to \frac{1}{a^2}(\langle\langle X\rangle\rangle - X) \tag{3.1}$$

where $\langle\langle X\rangle\rangle$ stands for the average over cells neighboring

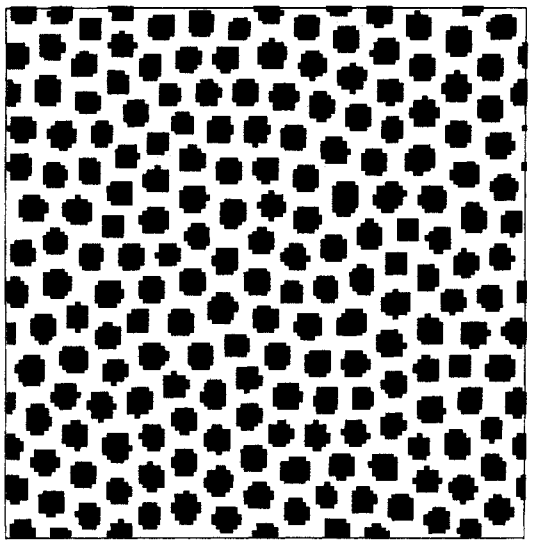

Figure 1. Domain pattern at $t = 10^4$ in the large system. The dark area denotes the region of $\psi > \bar{\psi}$.

the cell $\boldsymbol{n}$. For the present system, we used the following scheme:

$$\langle\langle X(\boldsymbol{n},t)\rangle\rangle = \frac{1}{6}\sum_{i\in\{N\}} X(i,t) + \frac{1}{12}\sum_{i\in\{NN\}} X(i,t) \quad (3.2)$$

where {N} and {NN} represent the nearest neighbor cells and the next nearest neighbor cells, respectively. Equation 2.9 is then transformed to the following difference equation:

$$\psi(\boldsymbol{n},t+1) = \psi(\boldsymbol{n},t) - \dot{\gamma} n_y \frac{1}{2}[\psi(n_x+1,n_y,t) - \psi(n_x-1,n_y,t)] + \langle\langle I(\boldsymbol{n},t)\rangle\rangle - I(\boldsymbol{n},t) - \alpha[\psi(n,t) - \bar{\psi}] \quad (3.3)$$

where $I(\boldsymbol{n},t)$ is the discrete version of the thermodynamic force $\delta H_S\{\psi\}/\delta\psi$ arising from the short range part of the free energy

$$I(\boldsymbol{n},t) = F(\psi(\boldsymbol{n},t)) - D[\langle\langle\psi(\boldsymbol{n},t)\rangle\rangle - \psi(\boldsymbol{n},t)] \quad (3.4)$$

In eq 3.3, the units of energy, length, and time are chosen in such a way that the lattice constant a and the transport coefficient M can be eliminated. The corresponding characteristic length and time scales in a real copolymer system are discussed below.

In the present simulation, we fixed the parameters as $f = 0.4$, $\alpha = 0.01$, and $D = 0.5$. The function $F(\psi)$ was chosen as $F(\psi) = -A\tanh\psi + \psi$ with $A = 1.3$. These choices result in disk-shaped equilibrium domains of radius $R \simeq 3$ locally ordered on a hexagonal lattice with domain separation $l \simeq 10$. Simulations were carried out for two different system sizes, 127×127 and 32×32, in order to check the system size dependence of the measured rheological properties. Examples of the equilibrium structure in the larger and smaller systems are shown in Figure 1 and Figure 2a, respectively. In the smaller system, an almost complete hexagonal lattice appeared, while the ordering was not complete in the larger system. The spatial dependence of $\psi(\mathbf{n})$ at $n_y = 10$ for the smaller system is shown as a function of n_x in Figure 2(b). We note that the interface separating A-rich and B-rich regions is rather diffuse in this case; for the parameters chosen above, the microphase-separated state is in the weak segregation regime.

In the weak segregation limit, the domain size is proportional to the radius of gyration R_G of a polymer chain in the disordered phase.[15] Since the domain size $R \simeq 3$, this implies that the cell size a is of the order of R_G; *i.e.* R_G is the physically relevant characteristic length scale. This also fixes the time scale (*cf.* eq 2.8); the corresponding physical time is the characteristic time of individual chain motion $t_{ch} \sim R_G^2/M$.

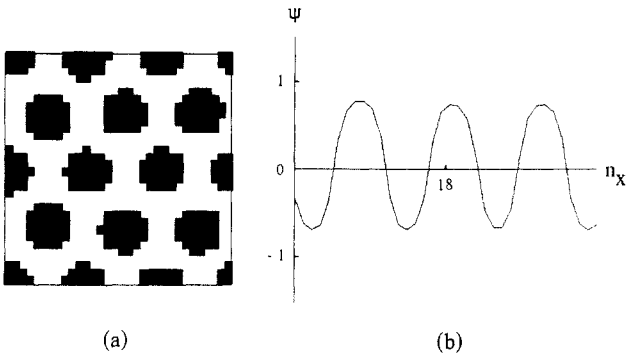

Figure 2. (a) Domain pattern at $t = 10^4$ in the small system. The dark area denotes the region of $\psi > \bar{\psi}$. (b) The concentration variation $\psi(\boldsymbol{n})$ along $n_y = 10$.

Our simulations involved a two-step procedure. First, we generated the equilibrium state by the following procedure. For each cell, we assigned a random number uniformly distributed between $\bar{\psi} - 0.125$ and $\bar{\psi} + 0.125$ and then solved eq 3.3 with $\dot{\gamma}(t) = 0$ for 10^4 time steps. Periodic boundary conditions were used in this procedure, so the condition

$$\psi(n_x,n_y,t) = \psi(n_x + N_xL, n_y + N_yL, t) \quad (3.5)$$

is satisfied for arbitrary integers N_x and N_y. The domain patterns shown in Figure 1 and Figure 2a were obtained in this way. We checked that these patterns do not change appreciably for longer runs up to 2×10^4 time steps.

After setting up the equilibrium structure, we applied the shear strain. In the smaller system, the applied shear is parallel to a hexagonal lattice basis vector. In the sheared state with strain $\gamma(t)$, the boundary condition becomes

$$\psi(n_x,n_y,t) = \psi(n_x + N_xL + \gamma(t)N_yL, n_y + N_yL, t) \quad (3.6)$$

for arbitrary integers N_x and N_y.

At each time step, we calculated the stress tensor using eq 2.10. To deal with the long range interaction term $G(\boldsymbol{r})$, we used a Fourier transform. Due to the sheared boundary condition, caution was required in the evaluation of the fast Fourier transform. In the present simulation, we made an Affine transformation for $\psi(\boldsymbol{r},t)$ at each time step and then calculated the Fourier component $\psi_{\boldsymbol{q}}(t)$ by

$$\psi_{\boldsymbol{q}}(t) = \int_0^L dx' \int_0^L dy\, \psi(x,y,t)\exp[i(q_x x + q_y y)] \quad (3.7)$$

where $x' = x - \gamma(t)y$. The vector $\boldsymbol{q}$ has components $\boldsymbol{q} = (2\pi/L)(m, n - \gamma(t)m)$ with m and n integers. The stress tensor $\sigma_{\alpha\beta}$ is then calculated from the Fourier components $\psi_{\boldsymbol{q}}(t)$ using

$$\sigma_{\alpha\beta} = -\frac{1}{L^4}\sum_{q\neq 0} q_\alpha q_\beta \left[D - \frac{\alpha}{q^4}\right]|\psi_{\boldsymbol{q}}(t)|^2 \quad (3.8)$$

4. Results

4.1. Oscillatory Strain. For the oscillatory flow, we considered frequencies ω in the range $10^{-4} < \omega < 10^{-2}$. If the frequency was higher than 10^{-2}, numerical instability took place, while if the frequency was lower than 10^{-4}, the computational time became prohibitively long. It should be noted that the frequencies in this range are much smaller than the characteristic relaxation rate of a single chain, the latter being of order unity in the units we employed. We have studied shear strain amplitudes $\Gamma = 0.1$ and 0.4

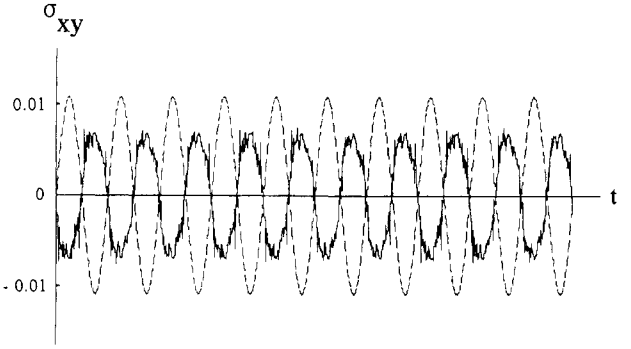

Figure 3. Time dependence of the shear stress σ_{xy} (solid line) in response to an applied oscillatory shear strain (dashed line). The unit of strain is arbitrary. To avoid overlap, $-\sigma_{xy}$ is plotted against t. The amplitude and the frequency of the shear strain are $\Gamma = 0.4$ and $\omega = 10^{-3}$, respectively. The data are taken from a simulation of the small system.

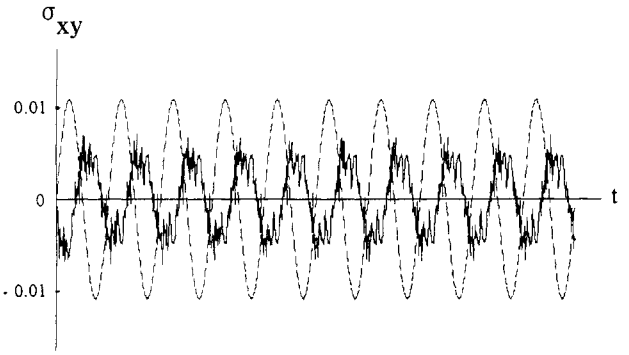

Figure 4. Time dependence of the shear stress σ_{xy} (solid line) in response to an applied oscillatory shear strain (dashed line). The amplitude and frequency of the shear are $\Gamma = 0.4$ and $\omega = 10^{-3}$, respectively, and the data are taken from a simulation of the small system. The style of the plot is the same as that in Figure 3.

in the large system and $\Gamma = 0.2$, 0.4, and 0.8 in the small system. Notice that the strains considered here are rather large. When the hexagonal lattice is sheared homogeneously, the deformation energy is maximum when the lattice becomes a rectangular one. The strain in this configuration is $1/\sqrt{3}$. Thus the strain $\Gamma = 0.8$ brings the lattice beyond this most unstable state. We carried out the simulation for up to ten periods of oscillation for each run. Steady state conditions were achieved in all cases except for the case of $\omega = 10^{-4}$ and $\Gamma = 0.4$ in the larger system, in which a gradual change of the stress with time was observed.

Figures 3 and 4 display the time dependence of σ_{xy} in the smaller system for $\omega = 10^{-3}$ and $\omega = 10^{-4}$, respectively, and for a strain amplitude of $\Gamma = 0.4$. For $\omega = 10^{-3}$, the time dependence of the stress is almost sinusoidal and in phase with the applied strain, indicating an essentially linear elastic response. On the other hand, for $\omega = 10^{-4}$ the stress deviates substantially from a pure sine curve and is shifted in phase from the applied strain. Qualitatively similar results have been obtained for the same values of Γ and ω independently of the system size, although the phase difference between stress and applied strain increases slowly with time in the large system.

In order to explore the stress–strain relation in detail, we have carried out simulations for $\Gamma = 0.2$, 0.4, and 0.8 and $\omega = 10^{-2}$, 10^{-3}, and 10^{-4} in the smaller system. The results are presented in Figure 5 as plots of the shear stress $\sigma_{xy}(t)$ against the shear strain $\gamma(t)$. We shall call such plots Lissajous patterns. The circulation is clockwise in these plots. Due to the small size of the system, there are

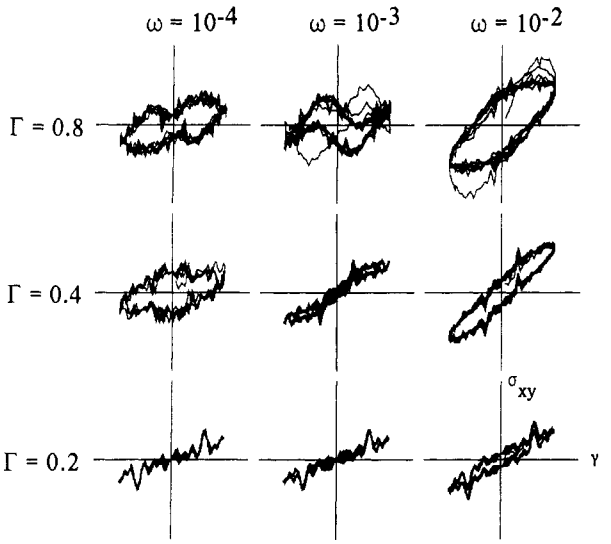

Figure 5. Lissajous pattern of the stress–strain relation in the small system. Note that the scale of the abscissa is adjusted for different values of Γ.

considerable fluctuations in the stress. However, one can see several general trends:

(1) For the small amplitude, $\Gamma = 0.2$, the curves are typical of the viscoelasticity of soft crystalline solids. At low frequencies $\omega = 10^{-4}$ and 10^{-3}, the Lissajous patterns are essentially lines, indicating that the system responds as a pure elastic solid. On the other hand, the curve becomes elliptic for $\omega = 10^{-2}$, indicating an appearance of viscous component in the stress at higher frequency. The characteristic relaxation time of this viscoelastic response is estimated to be between 10^2 and 10^3 in our time units.

(2) For a larger amplitude, $\Gamma = 0.4$, some anomalous behavior appears. The Lissajous patterns for $\omega = 10^{-2}$ and 10^{-3} can be still interpreted in terms of the linear viscoelastic model in (1): at high frequency, $\omega = 10^{-2}$, the pattern is elliptic, while at lower frequency, $\omega = 10^{-3}$, the pattern becomes a line, which in this case is slightly bent at the extremities, indicating that there is a small nonlinear effect in the equilibrium stress–strain relationship. The unusual behavior is seen at the lowest frequency, $\omega = 10^{-4}$. Here the Lissajous pattern adopts a rather wide lozenge shape. Qualitatively similar behavior is obtained in the simulation of the large system. This result cannot be interpreted in the framework of linear viscoelasticity; it is clearly a nonlinear effect.

(3) At an even larger amplitude, $\Gamma = 0.8$, which is larger than the value $1/\sqrt{3}$ corresponding to the most unstable, rectangular configuration, the nonlinear effect becomes more apparent. The pattern is deformed even at the highest frequency, $\omega = 10^{-2}$. Furthermore, for lower frequencies, there even appears a region of negative slope near the center of the Lissajous pattern.

In the next subsection, we will show that the anomalous Lissajous patterns are associated with the slippage of the lattice planes.

The Lissajous patterns for $\Gamma = 0.4$ in the large system are shown in Figure 6. One can see that the frequency dependence of the stress–strain curves is qualitatively similar to that in the small system, although the nonlinear effects for the case of $\omega = 10^{-4}$ are less pronounced.

Normal stress components were also calculated from the simulation data. Figure 7 shows the time evolution of the first normal stress difference,

$$N(t) = \sigma_{xx} - \sigma_{yy} \tag{4.1}$$

for the case of $\Gamma = 0.4$ and $\omega = 10^{-3}$. Since the normal

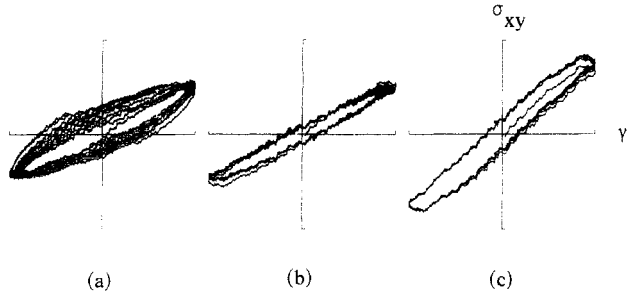

Figure 6. Lissajous pattern of the stress–strain relation for $\Gamma = 0.4$ and (a) $\omega = 10^{-4}$, (b) $\omega = 10^{-3}$, and (c) $\omega = 0.8 \times 10^{-2}$. The data are taken from a simulation of the large system.

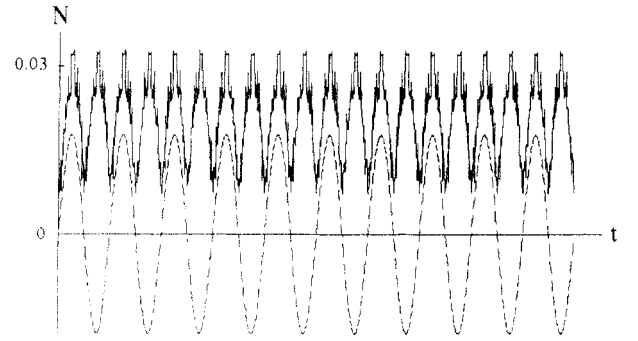

Figure 7. Time dependence of the normal stress $N(t)$ (solid line) in response to an oscillatory shear strain (dashed line). The amplitude and the frequency of the shear strain are $\Gamma = 0.4$ and $\omega = 10^{-3}$, respectively. The data are taken from a simulation of the small system.

stress is a second order nonlinear effect, it has a periodicity of π/ω, *i.e.* half the periodicity of the applied strain. Notice that $N(t)$ is positive and is rather large. For example in the case of strain $\Gamma = 0.4$, the ratio of the amplitude of $N(t)$ to that of $\sigma_{xy}(t)$ is approximately 4.5. This is in clear contrast to the normal stress effect in homogeneous polymer melts, in which the corresponding ratio is approximately 0.4.[31,32] Such large positive normal stress is understandable in these mesophase systems: large shear deformations of an ordered structure result domain overlap, which is relieved by the vertical motion of domains. This tendency toward vertical domain displacement leads to large positive normal stresses.

4.2. Step-Strain. To understand the unusual behavior of the Lissajous patterns, we carried out computer simulation for an applied step-shear. We started with the equilibrium configuration shown in Figure 2a and imposed a uniform shear strain γ at time $t = 0$. This was done by transforming the equilibrium configuration $\psi_{eq}(n_x,n_y)$ to $\psi'(n_x,n_y) \equiv \psi_{eq}(n_x - \gamma n_y,n_y)$. Thus, after the application of the shear strain, $\psi(\boldsymbol{n},t)$ satisfies the sheared periodic boundary condition in eq 3.6. The relaxation of the system was then simulated by using the time evolution equation (3.3) with $\dot{\gamma} = 0$. The sheared boundary condition was used during the entire relaxation process to ensure that the macroscopic strain was held constant.

In Figures 8 and 9, the relaxation of the shear stress σ_{xy} is shown for several values of the strain. When the applied strain is small ($\gamma = 0.1, 0.3$), the stress relaxes to the final stationary value with a relaxation time of about $\tau = 10^2$, which corresponds to that obtained for small strains in the oscillatory case. On the other hand, when the applied strain is large ($\gamma = 0.4$), unusual behavior is observed. After the initial relaxation at $t \simeq 10^2$, the stress level remains stationary for a significant period of time and then starts to decrease again at $t \simeq 1.2 \times 10^4$. In the smaller system, the second stress relaxation is quite sharp

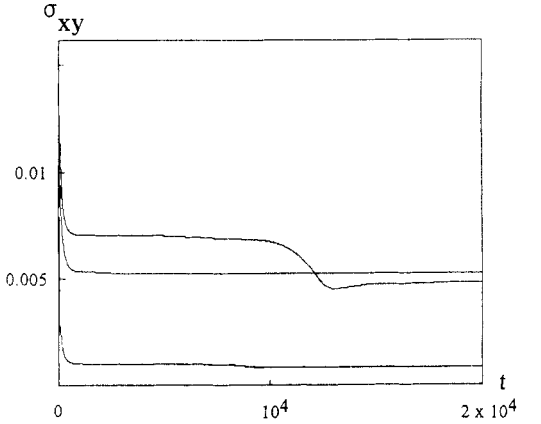

Figure 8. Time evolution of the shear stress σ_{xy} in the small system after the application of a step-strain. The applied strains are $\gamma = 0.4$, 0.3, and 0.1 from top to bottom.

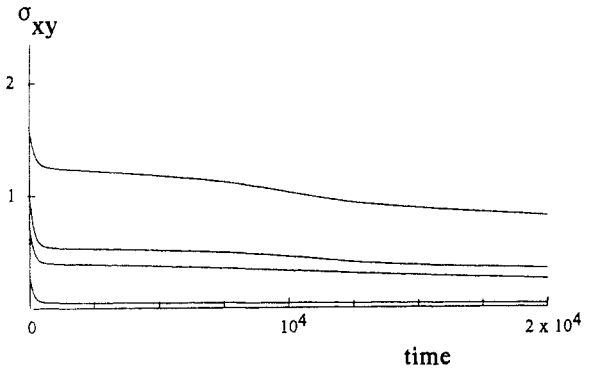

Figure 9. Time evolution of the shear stress σ_{xy} in the large system after the application of a step-strain. The applied strains are $\gamma = 0.6$, 0.4, 0.3, and 0.1 from top to bottom. The scale of the ordinate is normalized so that the initial value of σ_{xy} is unity for $\gamma = 0.4$.

and is accompanied by a slight stress undershoot. The second relaxation time is dependent on the initial domain structures and varies between 10^3 and 10^4 time steps. In the larger system, the second stress relaxation is quite gradual, as can be seen in Figure 9. Nevertheless, there is a clear double step relaxation in this case as well. The stress relaxation behavior is even more complex for $\gamma = 0.8$, in which case the stress becomes negative in the smaller system; in this case the system has been deformed beyond its most unstable state, $\gamma = 1/\sqrt{3}$.

Figure 10 shows the mesophase structural evolution during the course of the stress relaxation for $\gamma = 0.4$. Just after the strain is imposed, the domains are deformed, and the lattice is deformed from a hexagonal to a rectangular one (Figure 10a). The domain deformation quickly relaxes in a time scale of the order of 10^2. However, each domain is still distorted (slightly elongated along the x-direction) even at 5000 time steps (Figure 10b). Figure 9 indicates that the lattice relaxation occurs between $t = 10^4$ and 1.5×10^4. What has happened in this time interval is a relative slippage of layers in the shear direction. By comparison of the configuration of domains in Figures 10c and 10d, one can see that the layer indicated by A has moved to the right while the layer B has moved to the left, indicating slippage between planes A and B. The lattice at $t = 1.5 \times 10^4$ (Figure 10d) is still not a regular hexagonal lattice since that is incompatible with the boundary condition in the sheared state. It is this residual distortion of the lattice from the regular state that is responsible for the non-zero stress level for $t \to \infty$.

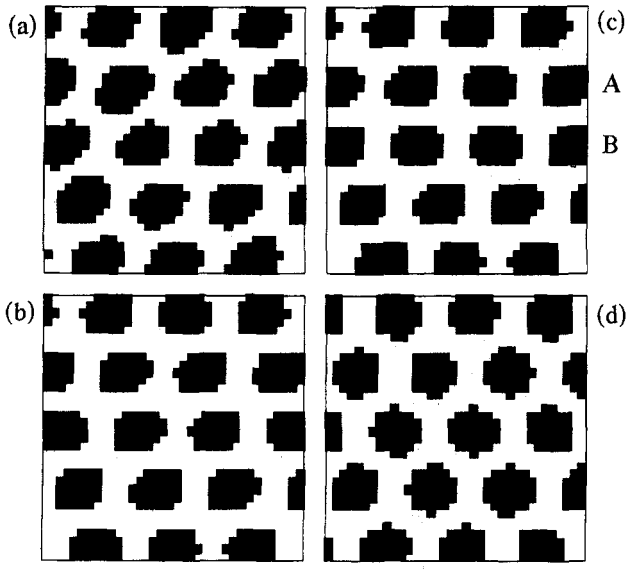

Figure 10. Evolution of the domain patterns in the relaxation process after the application of a step-shear: (a) $t = 1$ (the pattern immediately after the shear is applied), (b) $t = 5000$, (c) $t = 10\,000$, and (d) $t = 15\,000$. In order to aid in the identification of the domains under the sheared boundary condition, two extra cells are added at the boundaries.

5. Discussion

The present simulation indicates that there are two relaxation processes in the cylindrical mesophase of microphase-separated diblock copolymer under shear flow. One is the shape relaxation of each domain, which takes place with a relaxation time of about $\tau = 10^2$ in our time units. The other is a lattice relaxation via slippage which occurs on time scales of the order of $t = 10^4$. In real systems, there is of course a third relaxation mechanism due to chain entanglement, as in the case of any polymer liquid, but this process has a time scale much shorter than those considered here and has been neglected in the present model.

The first relaxation process takes place for any strain, while the second process appears only when the applied strain is large. For example, in the case of step-strain, the lattice remains distorted uniformly if the external strain is small. However if the external strain becomes large, the lattice reduces its distortion energy by relative slippage of layers, resulting in the anomalous double stress relaxation (*cf.* Figure 8). In the case of oscillatory shear strains of sufficient amplitude, the slippage of lattice planes results in the lozenge-shaped Lissajous patterns. In the following paper of this volume, we will present a phenomenological theory that reproduces the salient features of the anomalous oscillatory and step-strain behavior observed in this simulation, and that clarifies the connection between nonlinear rheological behavior and structural relaxation through the slippage of macrolattice planes.[33]

The phenomenon of lattice slippage suggests that the microphase-separated domain structure exhibits a kind of plasticity for large strains. Unlike the plasticity of metals, we did not observe the creation of defects and their subsequent propagation. Rather we observed that all domains belonging to a given lattice plane move in concert, resulting in the slippage of the lattice plane as a whole. Whether there exists an essential difference in the mechanism of plasticity between metals and block copolymer mesophases is an important question to be addressed in a future study. At this point, we note that there are several differences between block copolymer macrolattices and the usual small molecule crystalline solids. First, the fundamental unit of the block copolymer mesophase is a polymer micelle, which is a relatively large and soft object. Second, the block copolymer macrolattices exist in a very viscous environment, so the motion of defects takes place very slowly. In contrast, the defect motion takes place with the sound velocity in an atomic crystal. Considering these differences, it is not surprising that another mechanism may be playing an important role in the plastic deformation of block copolymer macrolattices.

Experimentally, it is well-known that rheological properties are very sensitive to the appearance of ordered phases. Indeed the ordered state is signified by the appearance of very nonlinear stress–strain patterns and very long relaxation times. The lozenge-shaped Lissajous patterns like those reported above, for instance, have been observed in rheological studies of spherical mesophases of microphase-separated block copolymer solutions in selective solvents.[6-8]

Though these phenomena are qualitatively parallel to the phenomena described here, detailed comparison indicates several subtle differences. Experimentally, the nonlinearity appears even for strains as small as $\gamma = 0.1$, while in the present system, the nonlinearity appears for $\gamma \simeq 0.4$. Furthermore, the double step relaxation behavior indicated in Figure 8 has not yet been observed experimentally. These discrepancies may be explained by the fact that real systems include substantial structural disorder, while in the present simulation (particularly in the small system), the crystalline order is nearly perfect. Indeed, in the simulations of the large system, which are substantially more disordered, the nonlinear effects in the oscillatory stress–strain relation and the double stress relaxation after a step-strain are much less pronounced. We also note that these discrepancies may be due to some intrinsic structural differences between the molten block copolymer mesophases we have considered here and the copolymer solution mesophases considered in the experiments. The experimentally studied mesophases consisted of dense spherical cores of precipitated blocks of the immiscible species in an entangled solution of the dissolved cilia of the second species, while the mesophases considered in our work are molten cylindrical phases of pure block copolymer in the weak segregation limit with no difference in flexibility between the two blocks. We expect that, by accounting for these structural differences and the disorder inherent in a macroscopic sample of mesophase, the discrepancy between the experiments and the simulations may be minimized. Of course, further study is needed to clarify these points.

Acknowledgment. We are grateful to Dr. H. Watanabe for informative discussions and to Dr. Y. Taguchi for useful comments on a related problem, through which we became aware of the necessity of an Affine transformation in the evaluation of the macroscopic stress. This work was supported by Tokuyama Science Foundation. J.L.H. was supported by a postdoctoral fellowship from the Japan Society for the Promotion of Science.

References and Notes

(1) *Developments in Block Copolymers-1*; Goodman, I., Ed.; Applied Science: New York, 1982 (see also references therein).
(2) Bates, F. S.; Fredrickson, G. H. *Annu. Rev. Phys. Chem.* **1990**, *41*, 525.
(3) *Block Copolymers: Science and Technology*; Meier, D. J., Ed.; MMI Press/Harwood Academic Publishers: New York, 1983.
(4) Hashimoto, T. In *Thermoplastic Elastomers*; Legge, N. R., Ed.; Hanser: New York, 1987.
(5) Kotaka, T.; White, J. L. *Macromolecules* **1974**, *7*, 106.

(6) Watanabe, H.; Kotaka, T.; Hashimoto, T.; Shibayama, M.; Kawai, H. *J. Rheol.* **1982**, *26*, 153.
(7) Hashimoto, T.; Shibayama, M.; Kawai, H.; Watanabe, H.; Kotaka, T. *Macromolecules* **1983**, *16*, 361.
(8) Watanabe, H.; Kotaka, T. In *Current Topics in Polymer Science*; Ottenbrite, R. M., Utracki, L. A., Inoue, S., Eds.; Hanser Publishers: New York, 1987; Vol. II, pp 61–96 (a review of experimental results).
(9) Bates, F. S. *Macromolecules* **1984**, *17*, 2607.
(10) Rosedale, J. H.; Bates, F. S. *Macromolecules* **1990**, *23*, 2329.
(11) Hugenberger, G. S.; Williams, M. C. *Macromolecules* **1988**, *21*, 1773.
(12) Kopi, K. A.; Tirrell, M.; Bates, F. S.; Almdal, K.; Colby, K. H. *J. Phys. Fr. II* **1992**, *2*, 1941.
(13) Larson, R. G.; Winey, K. I.; Patel, S. S.; Watanabe, H.; Bruinsma, R. *Rheol. Acta*, submitted for publication (and references therein).
(14) Helfand, E.; Wasserman Z. R. *Macromolecules* **1980**, *13*, 994.
(15) Leibler, L. *Macromolecules* **1980**, *13*, 1602.
(16) Hong, K. M.; Noolandi, J. *Macromolecules* **1983**, *16*, 1083.
(17) Semenov, A. N. *Zh. Eksp. Teor. Fiz.* **1985**, *88*, 1242; *Sov. Phys. JETP* **1981**, *61*, 733.
(18) Ohta, T.; Kawasaki, K. *Macromolecules* **1986**, *19*, 2621; **1990**, *23*, 2413.
(19) Kawasaki, K.; Ohta, T.; Kohrogui, M. *Macromolecules* **1988**, *21*, 2972.
(20) Kawasaki, K.; Kawakatsu, T. *Macromolecules* **1990**, *23*, 4006.
(21) Witten, T. A.; Leibler, L., Pincus, P. *Macromolecules* **1990**, *23*, 824.
(22) Rubinstein, M.; Obukhov, S. P. *Macromolecules*, in press.
(23) Kawasaki, K.; Onuki, A. *Phys. Rev. A* **1990**, *42*, 3664.
(24) Ohta, T.; Tetsuka, A.; Enomoto, Y.; Doi, M. In *Slow Dynamics in Condensed Matter*; AIP Conference Proceedings 256; Kawasaki, K., *et al.*, Eds.; AIP: New York, 1992.
(25) DeGennes, P. G.; *J. Chem. Phys.* **1980**, *72*, 4756.
(26) Joanny, J.-F.; Leibler, L. *J. Phys. (Paris)* **1978**, *39*, 951.
(27) Bahiana, M.; Oono, Y. *Phys. Rev. A* **1990**, *41*, 6763.
(28) Ohta, T.; Nozaki, H.; Doi, M. *J. Chem. Phys.* **1990**, *93*, 2664.
(29) Kasawaki, K.; Ohta, T. *Physica A* **1986**, *139*, 223.
(30) Oono, Y.; Puri, S. *Phys. Rev. A* **1988**, *38*, 434. Puri, S.; Oono, Y. *Phys. Rev. A* **1988**, *38*, 1542.
(31) Doi, M.; Edwards, S. F. *The Theory of Polymer Dynamics*; Oxford University Press: Oxford, U.K., 1986.
(32) Osaki, K.; Doi, M. *Polym. Eng. Rev.* **1984**, *4*, 35 and references therein.
(33) Doi, M.; Harden J. L.; Ohta, T. Following paper in this issue.